JOURNAL OF GEOPHYSICAL RESEARCH, VOL. 112, D10S03, doi:10.1029/2006JD007600, 2007

Airborne measurements of HCHO and HCOOH during the New England Air Quality Study 2004 using a pulsed quantum cascade laser spectrometer

Scott C. Herndon,[1] Mark S. Zahniser,[1] David D. Nelson Jr.,[1] Joanne Shorter,[1] J. Barry McManus,[1] Rodrigo Jiménez,[2] Carsten Warneke,[3] and Joost A. de Gouw[3]

Received 1 June 2006; revised 5 September 2006; accepted 11 October 2006; published 10 February 2007.

[1] Atmospheric mixing ratios of formaldehyde and formic acid have been measured from the NOAA WP-3 aircraft during the New England Air Quality Study (NEAQS) of July and August 2004 using a newly developed quantum cascade laser (QCL) spectrometer operating at a wavelength of 5.6 μm. The laser operates in pulsed mode with thermoelectric cooling. The detection is based on direct absorption in a compact 76-m multiple pass absorption cell. The laser is swept over a 0.5 cm^{-1} spectral region containing multiple lines of both HCHO and HCOOH. Absolute concentrations are retrieved by simultaneous spectral fitting routines with a detection limit (2σ) for HCHO of 0.3 parts in 10^9 (ppbv) with an averaging time of 60 s under stable flight conditions. HCHO mixing ratios in the range from 0.3 to 5 ppb were encountered during flight conditions. Some of the highest mixing ratios of HCHO were observed over heavily vegetated areas of Florida during the test flights where the ratios of HCHO to methacrolein and methyl vinyl ketone, measured by proton transfer mass spectroscopy, are consistent with formaldehyde production by isoprene oxidation. The highest mixing ratios of HCOOH, up to 10 ppbv, were observed in an aged forest fire plume encountered over northern Canada, in which ratios of HCOOH/CO are greater than previous observations, while the ratios of HCHO/CO are less than previous reports from forest fire plumes. Observations of HCHO/CO and HCOOH/CO in urban plumes are indicative of a mixture of sources from direct emissions and secondary oxidation of anthropogenic and biogenic hydrocarbons. The ability to measure both HCHO and HCOOH simultaneously is of value in assessing the oxidation mechanisms of atmospheric hydrocarbons and secondary organic aerosol formation and oxidation.

Citation: Herndon, S. C., M. S. Zahniser, D. D. Nelson Jr., J. Shorter, J. B. McManus, R. Jiménez, C. Warneke, and J. A. de Gouw (2007), Airborne measurements of HCHO and HCOOH during the New England Air Quality Study 2004 using a pulsed quantum cascade laser spectrometer, *J. Geophys. Res.*, *112*, D10S03, doi:10.1029/2006JD007600.

1. Introduction

[2] Atmospheric formaldehyde (HCHO) is a hydrocarbon photo-oxidation product as well as a HOx radical precursor [*Atkinson*, 2000; *Finlayson-Pitts and Pitts*, 2000]. In the remote clean troposphere it is formed mainly via the oxidation of methane, but in the terrestrial boundary layer oxidation of isoprene can dominate HCHO production [*Trainer et al.*, 1987]. Other sources may include the oxidation of secondary organic aerosol (SOA) as well as direct emissions from combustion sources including biomass burning, jet aircraft engines, compressed natural gas buses, and gasoline vehicles without a functioning oxidation catalyst. The photochemistry of HCHO can be used to constrain model predictions of HOx formation.

[3] Formic acid (HCOOH) sources in the atmosphere include isoprene oxidation, biogenic emissions and biomass burning [*Khare et al.*, 1999]. A considerable uncertainty, however, in the atmospheric fate and production schemes results when model data is compared to measured gaseous mixing ratios [*von Kuhlmann et al.*, 2003]. Experimental evidence suggests that the atmospheric oxidation of organic aerosol yields gas phase HCOOH and HCHO [*Molina et al.*, 2004]. Measurements of HCOOH in forest fire plumes potentially corroborate the speculation that HCOOH may be produced from the atmospheric processing of aerosol. *Mason et al.* [2001] and *Goode et al.* [2000] report anomalous behavior in the measured versus predicted HCOOH/CO ratio in the evolving plume. Though the gas-phase cycling of HCOOH holds some uncertainty, HCOOH may be an indicator of atmospheric oxidation of SOA.

[1] Aerodyne Research Inc., Billerica, Massachusetts, USA.
[2] Department of Earth and Planetary Sciences, Harvard University, Cambridge, Massachusetts, USA.
[3] Earth System Research Laboratory, NOAA, Boulder, Colorado, USA.

0148-0227/07/2006JD007600$09.00

[4] Both HCHO and HCOOH are important in understanding the formation and lifetime of SOA resulting form the oxidation of volatile organic compounds [*Andreae and Crutzen*, 1997; *Atkinson*, 2000; *Jacob and Wofsy*, 1988; *Rasmussen*, 1972; *Trainer et al.*, 1987; *Went*, 1960]. In an urban context, both the ozone and particulate matter represent potential health hazards [*Finlayson-Pitts and Pitts*, 2000]. In the troposphere, both ozone and aerosol contribute to the radiative forcing of Earth's climate [*Houghton et al.*, 2001]. A greater understanding of the mechanisms involved in photochemical ozone formation, atmospheric sulfur oxidation, and SOA formation, are necessary for understanding global climate change. Because SOA formation results from the photochemical processing of precursor gases, HCHO is an important indicator of aerosol formation and processing in an aging air mass [*Claeys et al.*, 2004; *Matsunaga et al.*, 2005]. Simultaneous measurements of both HCHO and HCOOH can provide information for improved models of SOA formation and transport. Gas phase measurements of formaldehyde are crucial to understanding the photochemical state of an air mass. Together with other measurements, these species challenge our modeled understanding of several atmospheric processes including ozone formation, the magnitude and partitioning of HOx [*Heard et al.*, 2004], the partitioning of oxidative capacity from the gas phase to the liquid phase, organic aerosol formation and secondary aerosol chemistry.

[5] Measurements of HCHO on airborne platforms have been pioneered by Alan Fried and coworkers using tunable diode laser absorption spectroscopy [*Fried et al.*, 1997, 1998, 2002]. Infrared laser absorption is one of the most sensitive and selective direct methods for detecting small molecules in the atmosphere and is particularly well suited for HCHO. The development of smaller, lighter, autonomous instrumentation would allow measurements from a wider variety of airborne and ground-based platforms. Recent advances in infrared laser technology using quantum cascade (QC) lasers allow the resulting instrumentation to operate without cryogenic cooling. Using lasers that operate in the 5.6 micron wavelength region, a single laser may be used to simultaneously measure both HCHO and HCOOH.

[6] This paper describes our first deployment of a non-cryogenic QC laser spectrometer aboard the NOAA WP-3 aircraft during the New England Air Quality Study (NEAQS) of 2004. This paper describes the instrument operation and performance, and presents measurement observations for HCHO and HCOOH.

2. Measurement Description

2.1. Instrumental Approach and Method

[7] The detection method was based on Tunable Infrared Laser Differential Absorption Spectroscopy (TILDAS) [*Fried et al.*, 1997; *Wagner et al.*, 2001; *Zahniser et al.*, 1995]. TILDAS has been used extensively for rapid, sensitive and selective detection of light trace gas species in laboratory, terrestrial, tower flux and airborne measurements. The laser sources for the measurements described in this study were thermoelectrically cooled, pulsed quantum cascade lasers (QCLs).

[8] The dual-QCL spectrometer combines pulsed quantum cascade (QC) lasers, an optical system, and a computer-controlled data acquisition system that incorporates the electronics for driving the two QC lasers along with signal generation and signal acquisition. The spectrometer is designed for simultaneous measurement of absorption (sample), pulse normalization (reference) and frequency lock spectra from two QC lasers. A key feature of the optical design is that the two laser sources are propagated along nearly identical optical paths and are cofocused onto the same detector elements. This greatly reduces the optical complexity. The signals from the two lasers are distinguished by temporal multiplexing; when one laser is pulsed, the other is suppressed. The timescale for alternating lasers is approximately 200 μs which is much faster than the time response of the gas sampling cell.

[9] We use commercially available distributed feedback (DFB) InGaAs-AlInAs/InP QC lasers designed for pulsed operation at near room temperature (Alpes Lasers, Neuchâtel, Switzerland). All the QC lasers that we used were single mode. Molecular transition selection for a given laser is achieved by temperature tuning, typically within -40°C to $+40^{\circ}$C using a two-stage Peltier element. The available spectral range (typically $\sim$6–14 cm^{-1} within 4–10 μm) is about $\sim$0.6% of the wavelength at 0°C. Since the lasers were operated in pulsed mode, they were subject to thermal frequency chirp during the pulse and had effective line widths of $\sim$0.008 cm^{-1} HWHM at 1765 cm^{-1}. This is slightly greater than the Voigt molecular line width for HCHO of 0.006 cm^{-1} HWHM at the sampling cell pressure of 40 Torr.

[10] Spectral scans were obtained by repetitively pulsing the lasers while simultaneously applying a subthreshold current ramp through a bias T. The lasers were excited with $\sim$13 ns electrical pulses typically repeated at 1 MHz ($\sim$1–2% laser duty cycle). The software-generated ramp modulated the laser temperature, and thus its spectral frequency across the target transitions. A fast (5 MHz) DAC/ADC board synchronously triggered the pulse electronics and integrated the resulting detector signals. The signal integration gate (50 ns) was matched to the detector response time ($\sim$60 ns rise time). The fast board also generated a TTL gate signal that defined the ramp duration, including a laser off period ($\sim$10 pulses) at the end of each sweep to measure the detector offset voltage. A typical spectral sweep consisted of 160–400 light pulses (160–400 μs at 1 MHz repetition rate), which implies a spectral sweeping rate of $\sim$2.5–7.0 kHz. The pulse trains sent to the two lasers were gated separately so that the spectral sweeps of the two lasers were interleaved.

[11] Figure 1 shows the layout of the optical system. The primary function of the optical system is to collect light from the two QC lasers and to direct it through an astigmatic multiple pass absorption cell (path length = 76 m, volume = 0.5 l) and onto a dual liquid nitrogen cooled HgCdTe photovoltaic detector. We use a reflecting microscope objective (15×, NA 0.5) for collecting the highly divergent elliptical (typically $\sim$60° vertical, $\sim$40° horizontal) QC laser beam. We have found that microscope objectives, although comparable to aspheric lenses in terms of collection efficiency, are in most cases superior regarding beam quality. This is particularly important for spectro-

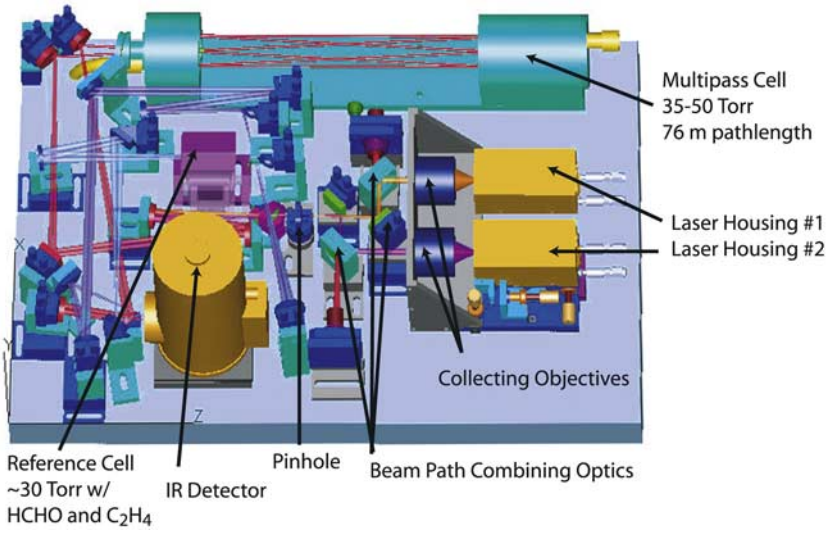

Figure 1. Dual pulsed quantum cascade laser optical table. The figure depicts the component layout with selected elements labeled. Through the use of beam combining optical elements, the two lasers are temporally multiplexed on a timescale much faster than the volumetric flow through the multipass cell. This instrument model allows ''simultaneous'' detection at two wavelengths.

scopic applications requiring relatively long optical paths. The optical table dimensions are 63 cm by 43 cm. The optical table is enclosed by a rigid aluminum cover when in use and is thermally stabilized by heating elements attached to the base of the optical table and to the aluminum cover. The optical design has been discussed in greater detail previously [*Jimenez et al.*, 2005].

[12] The operation of the spectrometer was fully automated and computer-controlled through *TDLWintel* [*Nelson et al.*, 2002, 2004], a Windows-based proprietary software package developed at ARI. *TDL Wintel* retrieves, analyzes, and stores the spectra along with housekeeping data. Concentrations are real-time determined from the spectra through a nonlinear least squares fitting algorithm (Levenberg-Marquardt) that uses the best available spectral parameters from the literature. The data analysis procedure includes pulse normalization of the sample (multipass cell transmission) spectra by dividing each spectral point from the sample cell by the corresponding signal from a second optical path that bypasses the sampling cell in order to reduce the variations in pulse-to-pulse intensity from the laser [*Nelson et al.*, 2002, 2004]. Each 1-s normalized spectrum is then divided by an averaged background spectrum recorded in the same sampling cell but with HCHO-free air (described below). The resulting spectra are fitted in real time using a low-order polynomial for the spectral baseline and convolving the laser line shape with the molecular Voigt absorption line shape calculated from the known pressure and temperature of the sampling cell and a molecular line transition database. Computational speed is optimized by using approximations to the Voigt profile [*Humlicek*, 1979, 1982] and assuming a Gaussian model for the laser line shape.

[13] This campaign was the first application of pulsed quantum cascade laser technology in an airborne platform. Example flight spectra are shown in Figure 2. These spectra are 5 min averages of data obtained on the transit flight of 5 July 2004. The circles are the data points, and the lines are the result of the nonlinear least squares fits to the data. The first laser operated near 1765 cm^{-1} and monitored formaldehyde and formic acid, while the second laser operated near 967 cm^{-1} and detected ammonia. The data acquisition system devoted 160 channels (laser pulses) to the total sweep cycle. The total sweep rate was 6.25 kHz where the sweep cycle consisted of 100 channels for the HCHO/HCOOH laser, 50 channels for an NH_3 laser and 10 channels with pulses suppressed, devoted to the measuring the zero-light level. Coadded spectra were collected each second, archived and processed according to Beer's law absorptions. The instrument was configured with these two lasers during the initial deployment. An inopportune failure of the 1765 cm^{-1} laser after the initial three flights, necessitated the use of replacement lasers which accessed less optimal spectral regions at 1775, 1779 or 1782 cm^{-1} during the remaining flights. We therefore operated only one laser channel of the instrument to maximize the duty cycle for detecting just formaldehyde and formic acid on the flights conducted after 12 July 2004.

2.2. Spectroscopic Detection of Formaldehyde in the ν_2 Absorption Band

[14] An ideal wavelength to detect formaldehyde is in the ν_2 band at 1765 cm^{-1}. The peak absorption depth of a 43 Torr, 1 ppbv mixture of HCHO with a laser line width of 0.008 cm^{-1} is $\sim 4 \times 10^{-5}$. In the $\nu_1 + \nu_5$ band (just below 2832 cm^{-1}), the equivalent absorbance of a strong feature is only 2×10^{-5}. Though this represents an advantage in absorption depth for the ν_2 band over the $\nu_1 + \nu_5$ band, there is a potential limitation in the presence of stronger water absorption lines. Figure 3 illustrates these tradeoffs.

[15] Figure 3 shows three simulated transmission spectra in the ν_2 band (Figures 3a–3c) and one spectrum in the $\nu_1 + \nu_5$ band (Figure 3d) for comparison. The vertical bar represents an absorbance of 2×10^{-5} in each of the spectra (Figures 3a–3d). In order to minimize the demands placed

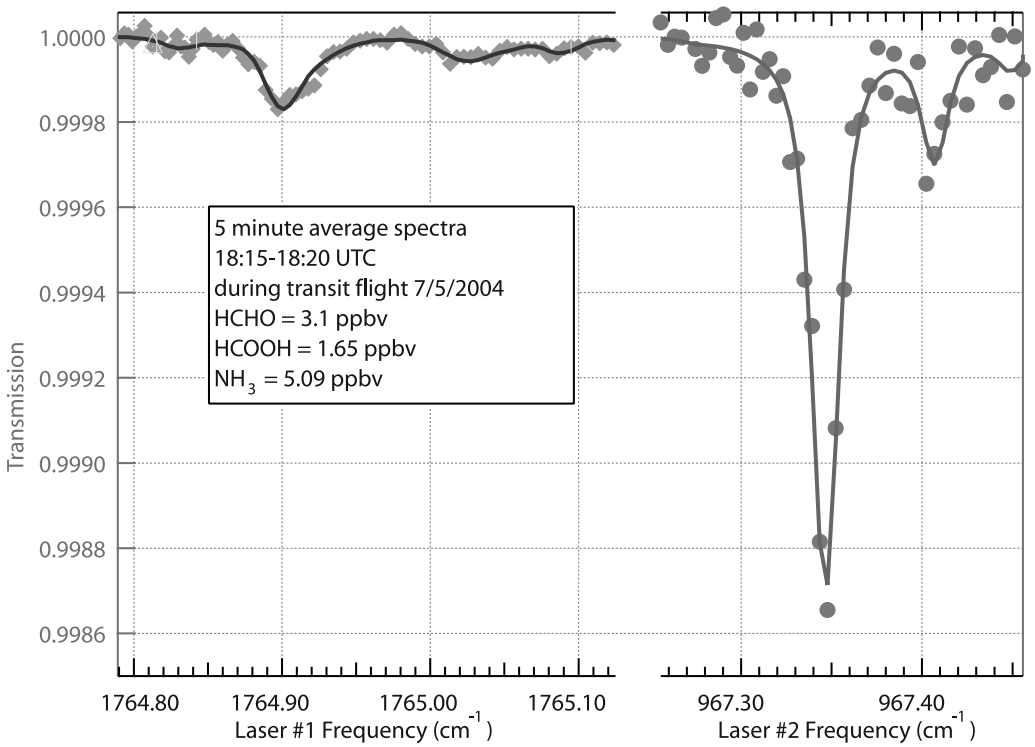

Figure 2. Dual laser sweep. The figure shows a 5-min averaged spectrum for the initial configuration during this mission. The 1765 cm^{-1} laser is used to measure HCHO and HCOOH while the 967 cm^{-1} laser is measuring NH_3.

on the spectroscopic model used for the "wings" of the water absorption lines, we used a humidity matching, zero-air generator to obtain spectra with most of the water absorbance cancelled out. The details of this component of the instrument are given later. Figures 3a and 3b show the simplification in the spectrum which results from reducing the humidity by a factor of ten. The water absorbance in each panel is the base absorption line, and the absorbance due to formaldehyde is the additional shaded area. Note that the influence of the water lines is greatly reduced in Figure 3b which allows more sensitive retrieval of formaldehyde concentrations.

[16] Figure 3c is similar to Figure 3b, except that the laser line width is negligibly small in this simulation. Note the sharpening of the spectral lines and the improved separation between the water and formaldehyde lines. This improved resolution may be achievable in the future as cw QC lasers, which are presently available at 1900 cm^{-1} [*McManus et al.*, 2006; *Nelson et al.*, 2006], become available in the 1765 cm^{-1} spectral region. Until recently, most cw QC lasers required cryogenic cooling but near room temperature operation is now being reported by several groups at many different wavelengths [*Bakhirkin et al.*, 2006; *Beck et al.*, 2002; *Blaser et al.*, 2005; *Moeskops et al.*, 2006; *Yu et al.*, 2005]. Figure 3c also shows a dashed trace. This shows the spectrum that would result if the sample pressure were reduced to 25 Torr to take advantage of the negligible laser line width. At this pressure, there is a modest reduction in peak absorbance but nearly complete separation between the water and formaldehyde lines. Figure 3d is similar to Figure 3c, except for the wavelength region. Comparing Figure 3d to Figure 3c shows the additional absorbance which is available in the ν_2 band. The simulations include the same differential water vapor of 0.13% corresponding to a factor of 20 reduction relative to the largest water vapor mixing ratios (3%) encountered under flight conditions. While there is more baseline curvature because of water at 2381 cm^{-1} in Figure 3d, the influence of water vapor on the fitting retrieval can be more pronounced in the 1765 cm^{-1} region because of the proximity of the smaller water vapor lines. Simultaneous fitting of HCHO and H_2O minimizes the effect of water vapor fluctuations. We observe less than 0.02 ppb HCHO for a 0.1% change in water vapor mixing ratio during in situ observations.

[17] Although the simulation of the ν_2 band in Figure 3 includes only spectral lines due to water and formaldehyde, formic acid (HCOOH) is also sufficiently active at this wavelength that is must be included in the spectroscopic concentration retrieval. In order to separate the spectra due to HCOOH and HCHO, the wavelength region needs to be expanded to include the HCOOH lines at 1765.0841 and 1765.092 cm^{-1}. These strong formic acid lines are well separated from the strong formaldehyde line at 1764.90 cm^{-1}, permitting a clean retrieval of both species under most conditions.

[18] Figure 4 shows a multiple species fit to flight data that retrieves HCHO in the presence of HCOOH. Figure 4 shows a flight spectrum acquired on 11 July 2004. This spectrum was constructed by averaging 30 min worth of individual flight spectra. As Figure 4 shows, the analysis procedure is able to decompose the spectrum into three

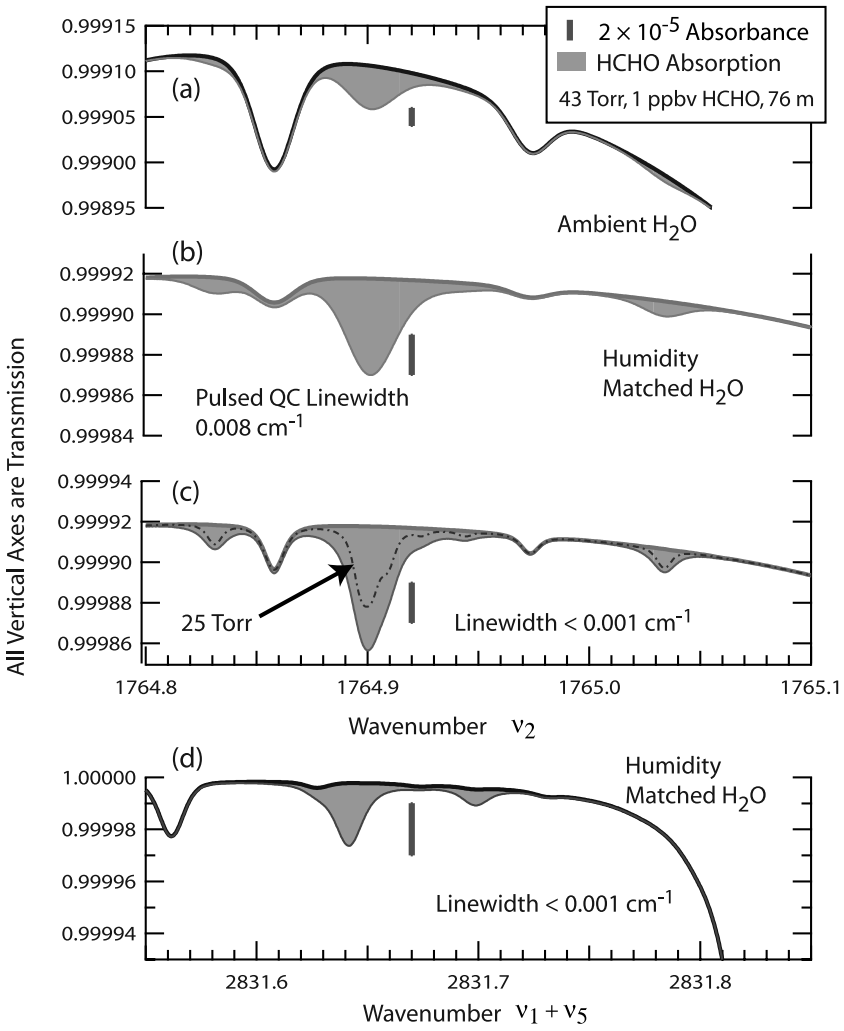

Figure 3. HITRAN simulations of HCHO absorptions at various wavelengths, conditions, and laser line widths. (a–c) Simulated transmission spectrum versus wave number for the ν_2 HCHO absorption band at 1765 cm^{-1} and (d) the same for the $\nu_1 + \nu_5$ band at 2381 cm^{-1}. The height of the vertical bar in each panel is equivalent to an absorption depth of 2×10^{-5}, to help guide the eye in comparing relative absorption depths between the spectra. Figures 3a and 3b are meant to show the effect of matching the humidity of the background air; 1.3% H_2O in Figure 3a versus 0.13% H_2O in Figure 3b. The effect of narrowing the laser line width from 0.008 cm^{-1} to 0.001 cm^{-1} is shown in the contrast between Figures 3b and 3c. Figure 3d shows that the absorption line at 1765 cm^{-1} is stronger than that at 2831 cm^{-1}.

components: formaldehyde (thick solid line), formic acid (thick shaded line) and Δ water (residual water after humidity matching, thin shaded line).

[19] The spectroscopic line parameters for formic acid are not as well studied as those for formaldehyde. We constructed an absolute spectroscopic model for formic acid in this region by combining recently measured high-resolution, relative intensities and spectral line positions for formic acid (J. Vander Auwera, Free University of Brussels, personal communication, 2004) with lower-resolution, quantitative spectra (Northwest Infrared Vapor-phase Spectral Library, http://www.pnl.gov). In this procedure, we carefully accounted for the instrumental line width in the lower-resolution spectrum and derived absolute line strengths and broadening coefficients. We estimate the accuracy of the resulting line strengths at ~20%. The cross interference of HCHO on the retrieval of HCOOH is +0.05 mol HCOOH per mole of HCHO as determined by in situ observations of HCHO plumes from combustion sources.

[20] Other potential spectroscopic interferences were evaluated. The interferences due to methanol, isopropyl alcohol, and acetaldehyde were characterized in the laboratory. The absorbance due to each of these species is less than 0.1% of the absorbance that would be produced by an equal mole fraction of HCHO. Furthermore, because the spectral profiles of these species are distinct from those of HCHO and HCOOH, the influence of these species on the retrieved concentrations will be even smaller. Laboratory measurements of the potential influence of other carbonyls on the retrieved HCHO mixing ratio have been planned.

2.3. Zero Air Generator

[21] We used the same design for the inlet sampling system and the zero air generator that has been developed

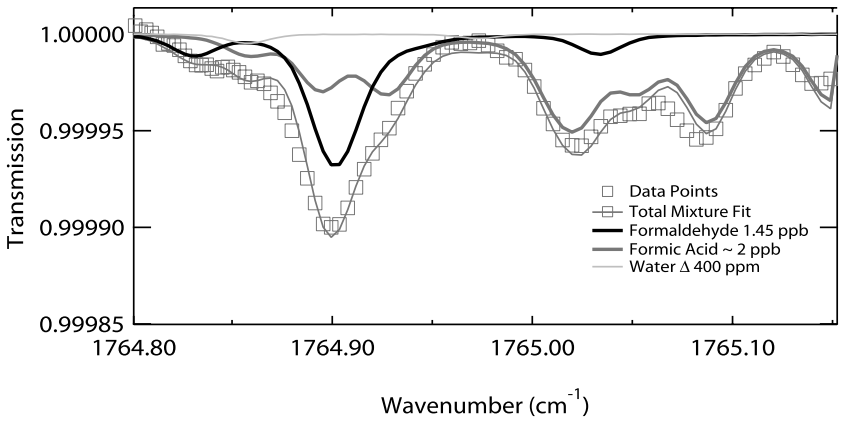

Figure 4. Multiple species fit to 30-min average spectrum. The squares are the acquired data points, and the shaded line is the composite fit. The subcomponents of the shaded line are shown: Solid indicates HCHO, thick shaded indicates HCOOH, and thin shaded indicates matched H_2O. The laser line width is being modeled by a 0.008 cm^{-1} gaussian in this fit.

by Fried for previous aircraft measurements of HCHO [*Fried et al.*, 1998]. A schematic diagram of the inlet system is shown in Figure 5. Outside air is sampled through a 1/2 inch outside diameter Teflon line which protruded 2 cm beyond a heated "winglet" which was mounted on an aluminum plate which replaced a window on the starboard side of the aircraft. The aerodynamically shaped winglet extended just beyond the boundary layer of the aircraft. Provisions for adding both "zero air" and calibration gas from a permeation source are included within the winglet 8 cm from the tip of the inlet. The tubing within the winglet assembly is heated to 40 C. The sample gas passed through a pressure controlled valve midway between the winglet and the absorption cell which adjusted automatically to maintain a pressure of 55 Torr down stream of the valve. This resulted in a constant pressure of 43 Torr in the sampling cell at a flow rate of 7.5 standard liters/minute regardless of the aircraft altitude. The flow rate was set

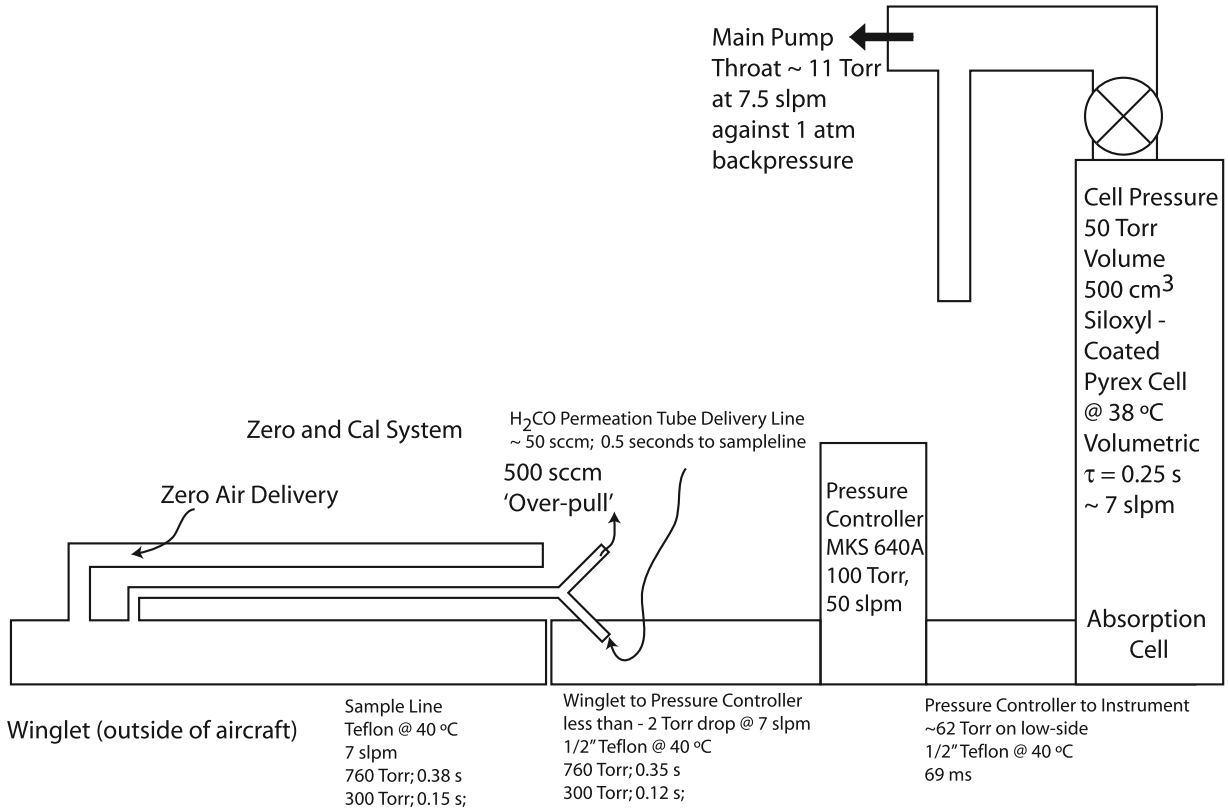

Figure 5. Schematic representation of the instrument sampling system. All noted residence times are estimated from bulk flow calculations. The pressure drops are estimated using the Poiseulle equation and the composition of a standard atmosphere.

initially by manually adjusting a ball valve between the sampling cell and a 600 liter/minute vacuum pump to obtain the predetermined operation pressure.

[22] The zero air generation system used ambient air collected outside the aircraft which is compressed with a diaphragm pump and passed through a palladium catalyst heated to 300 C to remove hydrocarbons. The basic premise is to continuously generate HCHO free air while matching humidity as closely as possible. Matching humidity is particularly valuable in the 1765 cm^{-1} spectral region where the wings of nearby water lines can add curvature to the baseline. In our differential absorption detection method, the effect of matching humidity reduces the order of the polynomial necessary to represent this curvature. Matching the humidity between sample and background also reduces the uncertainty introduced to the fitting procedure from our imperfect description of the laser line shape, especially in the wings of nearby water lines. We are able to monitor the effectiveness of matching the water vapor difference by observing the weak water lines in the vicinity of the HCHO and HCOOH features as shown in Figures 3 and 4. We generally can match the water to within 2% of its ambient value during stable flight conditions through air of constant humidity. However, there is a time lag on the order of several minutes for equilibration to changes in ambient water vapor that are encountered when the aircraft changes altitude or passes through clouds that create a mismatch between sample and background of up to 20% of the ambient level. Accurate retrieval of HCHO concentrations under these conditions in real time is compromised, although data may be recovered by postprocessing. The water vapor difference may also be used to exclude data during postprocess averaging.

[23] The efficiency of the hot catalyst in scrubbing HCHO was determined by introducing paraformaldehyde vapor into the zero air generator intake. This was done prior to the mission in the laboratory and also near the midpoint of the NEAQS campaign with the instrument integrated in aircraft at the hangar. The results indicate that over 99.9% of the HCHO is being removed by the catalyst using paraformaldehyde source. It is still possible that a highly unusual mixture of hydrocarbons could produce HCHO in the catalyst, but we see no evidence for this by challenging the catalyst with hydrocarbons in the laboratory.

[24] The optimum cycle time for zero air addition in a background-limited absorption measurement is to spend equal amounts of signal processing time on both the sample and the background, and to switch between sample and background as rapidly as possible within the response time of the instrument. The small volume (0.5 liters) of the multiple pass absorption cell allows a short time interval between sample and background measurements. At the flow rate and pressures used in the sampling cell, the time constant for exchange of gas in the cell is ~0.3 s. We used a cycle for switching between ambient air and "zero air" with 20 s total duration consisting of 7 s ambient sample, 7 s background "zero air," and 3 s of flushing time between sample and background. Spectra during the sample part of the cycle were saved at 1 s intervals and each spectrum was divided by the previously accumulated background spectrum before applying the spectral fitting algorithms. Thus the real time data consisted of 7 s of continuous data followed by a 13 s interval between samples. The mixing ratios are reported in real time in a data file and on the computer screen. All the spectra (data and background) are also saved to the computer's hard drive for post processing and spectral averaging.

2.4. Permeation Source of HCHO

[25] The spectroscopic method employed in these measurements has its accuracy tied to the measured line strengths [*Herndon et al.*, 2005b]. This spectroscopic accuracy, however, applies only to the sample in the absorption cell and does not address inlet losses. The most robust verification of inlet performance is achieved by characterizing transmission losses and response time using field standards [*Ryerson et al.*, 1999]. In order to verify the transmission of HCHO through the inlet, a permeation source is used. The permeation tube oven was constructed by Neuman [*Neuman et al.*, 2003]. The temperature of the permeation source (Kin-Tek, La Marque, Texas) was maintained at 333 K with an Omega temperature controller. The stated permeation rate provided by the manufacturer diluted into 7.5 slpm results in a predicted concentration of 6.9 ppb in the instrument. The instrument measurements of the calibration source during dedicated testing at the ground before and during the measurement campaign resulted in measurements of 6.85 ± 0.13 ppb. This permeation source was also checked using another instrument that employed a traditional lead-salt diode laser. The key differences in this other measurement were decreased flow rate (5.6 slpm versus 7.0 slpm) increased path length (210 m versus 76 m), decreased line width (<0.001 versus 0.008 cm^{-1}) and a increased volume (5 versus 0.5 liters). The lead-salt TDL measurement of the permeation source was lower by 3%. The accuracy of the line strengths used to measure HCHO in this wavelength region is 7% [*Herndon et al.*, 2005b]. The level of agreement between the predicted HCHO concentration from the permeation source and the measurements with the flight instrument indicates there were not significant losses of HCHO in the sample line. This result agrees with previous work characterizing the transmission of HCHO through Teflon sampling lines [*Wert et al.*, 2002].

[26] The response time of the whole inlet/instrument system was also measured using the permeation source. Figure 6 shows the resulting HCHO concentration in time as the output from the permeation source is added to the inlet. The inlet tip was flooded with zero air (8.1 cm from inlet tip) and the permeation source added just downstream (13.2 cm from inlet tip), see Figure 5. The zero air addition point along the main sample line allows for more than 6 tube diameters. This has been shown empirically to prevent ambient air from being dynamically entrained in the sample during a zero air purge [*Wert et al.*, 2002]. The lag time associated with the switching of the permeation source is measured to be 0.7 s while bulk flow calculations of the various components from the inlet to the instrument predicts 0.9 s. The response time, determined by exponential fitting to either of the rise or fall in concentration results in time constants of 0.35 s for the decay and 0.3 s for the rise. Plug flow calculations for the section of the absorption cell between the mirrors indicate that each time constant should be 0.25 s. The slightly increased response time is likely due to a combination of the dead volumes in the

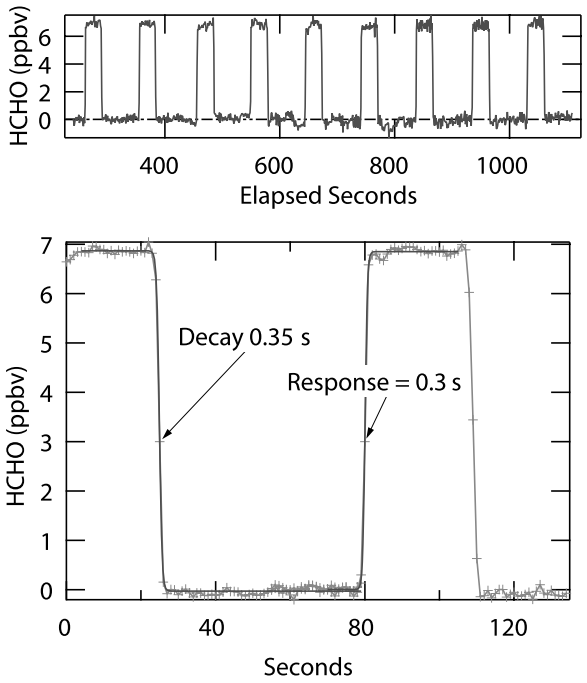

Figure 6. Measured transmission and response of permeation source of HCHO. (top) Measurement of HCHO as a function of time. The permeation source was alternately allowed to enter the inlet or be pulled away from the inlet by a solenoid controlled vacuum "overpull." (bottom) Result of fitting decay and rise times to an exponential function.

sampling cell located behind the mirrors and deviations from ideal plug flow within the cell. The allowance for 3 s of flushing time between sample and background corresponds to 10 e-folding times in cell response.

2.5. Fitting Averaged Spectra Versus Averaged Concentrations

[27] During the field campaign, spectra were typically analyzed and saved with a time resolution of 1 s. The software does the spectral fitting in real time and reports the concentrations immediately. Additional spectral signal averaging can be used to lower the detection limit and confirm that other potential absorbers in this wavelength region are not significantly influencing the extracted concentrations. In this spectral post processing, the collected 1-s spectra are processed using one of two algorithms: (1) simple coaddition or (2) coaddition with wavelength shifting. In the first algorithm the acquired spectra are averaged together without regard to the possibility of laser frequency drift. The second algorithm attempts to correct for frequency drift, by shifting the frequency scales of the saved sample spectra on the basis of the results of fits to synchronous reference spectra. These reference spectra were obtained simultaneously by monitoring a sealed reference cell with a large concentration of formaldehyde. The result of averaging with these two methods is shown in Figure 7.

[28] Figure 7a shows the location of the reference peak as a function of time. The spectral drift observed corresponds to a temperature drift of ~50 mK due to imperfect operation of the laser temperature controller. The 1765 cm^{-1} HCHO absorption feature was located at channel 47.5 in the early portion of this time series, but drifted to ~48.3 twelve minutes later. The effect of this temperature driven drift (0.8 channels or ~0.003 cm^{-1}) is apparent in the difference between the two post processing algorithms. Figure 7b shows the composite 5 min average spectra obtained using the two averaging methods (simple average in squares, frequency corrected average in shaded triangles). The effective laser line width of the spectrum obtained with simple averaging does not account for the wavelength drift and is unreasonably large (0.014 cm^{-1}) compared to the composite spectrum that was created with correction for frequency drift (0.009 cm^{-1}). Furthermore, the latter laser line width value more closely matches the measured laser line width derived from fits to nearby strong water lines (0.008 cm^{-1}) without spectral averaging. The more sophisticated averaging method maintains spectral resolution and provides additional assurance of the absence of spectral interference from other species. Though the laser line width used in the 1 s real-time fitting is not influenced by this phenomenon, when refitting the averaged spectra, a failure to account for the line position wandering during periods of excessive drift can result in retrieved concentrations which are low by up to 18%. Laser wavelength control has been improved considerably through the use of better temperature controllers in the current instrument.

[29] We also evaluated the difference between averaging the concentrations returned from fits to the 1 s spectra and averaging the 1 s spectra to produce a composite spectrum which was subsequently analyzed. A comparison of the average of the 1-s fit results (generated in real time) to the refit averaged spectra (generated during postprocessing) agree very well for all timescales; 1, 5 and 30 min and concentration ranges (<100 pptv–7 ppbv).

2.6. Additional Airborne Measurements

[30] This article focuses on the TILDAS instrument performance on board the NOAA WP-3 aircraft during the NEAQS-ITCT 2k4 campaign. The flights departed from Portsmouth, New Hampshire, US and were conducted between 5 July and 15 August of 2004. Of course, the TILDAS measurements were not made in isolation; the aircraft was equipped with an extensive instrument payload. In the following sections, we correlate our results with those obtained by other instruments which were also flown on this platform. One of these instruments is a Proton Transfer Reaction Mass Spectrometer (PTR-MS) which provides measurements of oxygenated volatile organic species. Its deployment aboard the aircraft has been described previously [*de Gouw et al.*, 2006]. In addition, we refer to carbon monoxide (CO) measurements that were performed using a vacuum ultraviolet fluorescence instrument [*Holloway et al.*, 2000].

3. Results and Discussion

3.1. Isoprene Oxidation Event

[31] Data from the test flight on 3 July 2006 show an interesting formaldehyde feature which resulted from the atmospheric oxidation of isoprene. The period of interest is shown as a time series along with data from the PTR-MS, in Figure 8. The time series shows a relatively low concentration of HCHO (166 pptv) while the aircraft was

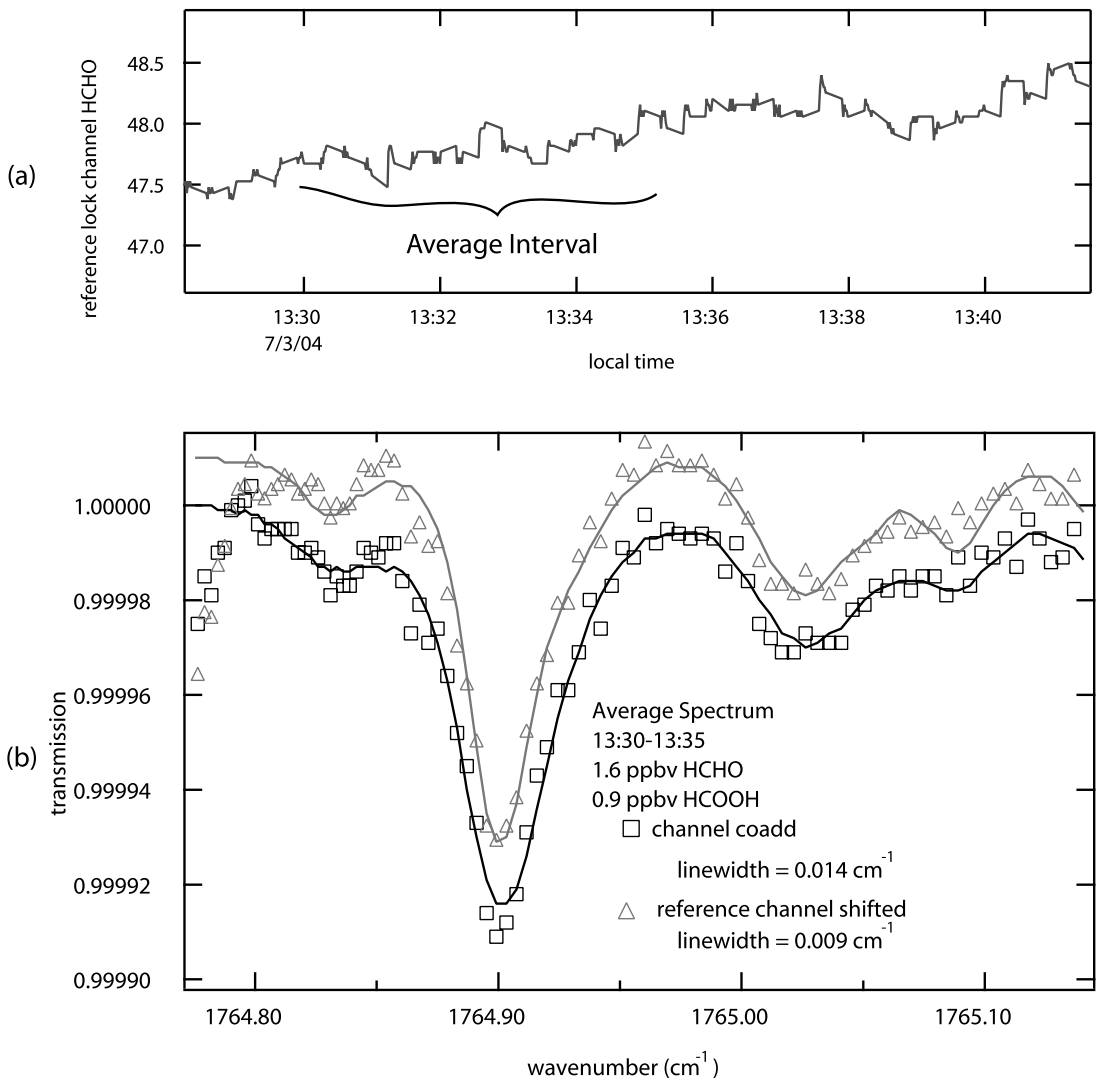

Figure 7. Five minute average spectra via two algorithms. (a) Drift in the reference lock channel number during a 14 min period (see text for additional detail). (b) Results of the spectroscopic averaging using an algorithm which averages the channels (depicted by the squares) and an algorithm which uses the reference lock frequency to shift the spectra prior to averaging (depicted by the shaded triangles). The shaded spectrum and data points have been offset for visual clarity by 1×10^{-5}.

at 2250 m. When the aircraft descended to 450 m at 1255 local time (LT) the concentration of HCHO rose sharply to 4.3 ppbv. The operator on the test flight noted we were flying above a heavily vegetated area with no visible roads. Abruptly, at 1305 LT we crossed into an urban area with no appreciable vegetation aside from grass and trees from residential areas. The cause of the increased HCHO is consistent with a rapid ($\sim$1 hr) oxidation of biogenic isoprene [*Li et al.*, 1994; *Palmer et al.*, 2003]. The presence of concomitant increases in Methacrolein (MACR) and Methyl Vinyl Ketone (MVK) corroborates the assertion that this is an isoprene oxidation event [*Orzechowska and Paulson*, 2005; *Zhao et al.*, 2004]. The relative ratio of HCHO to the sum of MVK and MACR in the first plume (1255 to 1307 LT) is 1.2 ± 0.2 and in the second plume (1342 to 1350 LT) is 2.4 ± 0.3, twice as large.

[32] The ratio of HCHO to the sum of MVK and MACR as first generation oxidation products for OH initiated isoprene oxidation ranges from 0.9 to 1.1 [*Miyoshi et al.*, 1994; *Sprengnether et al.*, 2002; *Tuazon and Atkinson*, 1990]. Though the ratio of HCHO to the sum of MVK and MACR is greater in the first generation products from the direct ozonolysis of isoprene [*Zhang et al.*, 2002], the local daytime conditions most likely favor the majority of the isoprene oxidation to be taking place via OH initiated oxidation [*Palmer et al.*, 2003]. Because the data shown in Figure 8 were collected during a test flight, many of the additional measurements needed to fully model these results may not be available. The difference in the observed HCHO to MVK/MACR sum between the two plumes as well as the difference in the isoprene to methanol ratio will be further investigated.

3.2. Fire Plume Intercept

[33] A fire plume was intercepted over northern Canada on the flight of 9 July 2004. Figure 9 shows the time series for this event. Relative to CO and acetonitrile, the abun-

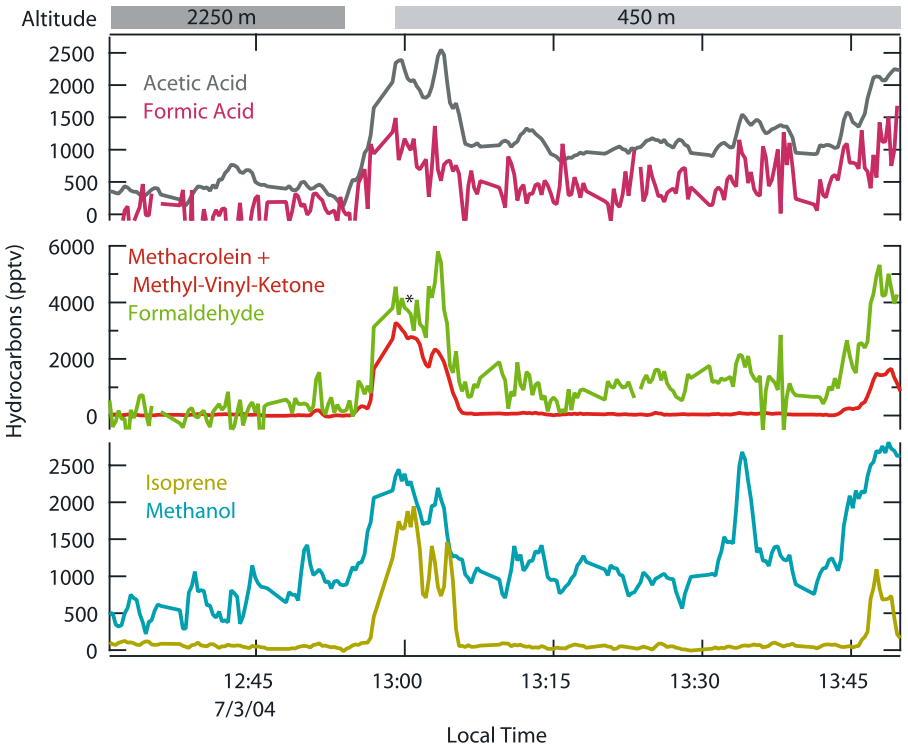

Figure 8. Isoprene oxidation event. The time series for several hydrocarbons is depicted from a test flight in the Tampa, Florida, area. Prior to 1300 LT, the WP-3 was level at 2250 m but then descended to 450 m. The methanol and isoprene plumes centered at 1300 LT mark the period of time when the aircraft was directly above a forested area. A subset of the oxidation products of isoprene is shown in the middle time series, the sum of methacrolein and methyl-vinyl-ketone as well as the measured formaldehyde.

dances of HCHO are lower than are measured in most "fresh" fire plumes by an order of magnitude [*Goode et al.*, 2000; *Mason et al.*, 2001]. The FLEXPART transport model was used to calculate back trajectory fields along the aircraft flight track [*Stohl et al.*, 2003]. The back trajectory calculations of this plume intercept indicate that the air mass was heavily influenced by emissions from a surface fire 8 ± 2 days prior [*de Gouw et al.*, 2006]. The implication is that directly emitted HCHO was not as elevated as observed in fresh fire plumes because of its short photochemical lifetime of a few hours, and the observed HCHO was likely in photochemical equilibrium from the slow oxidation of other hydrocarbons in this "aged" fire plume.

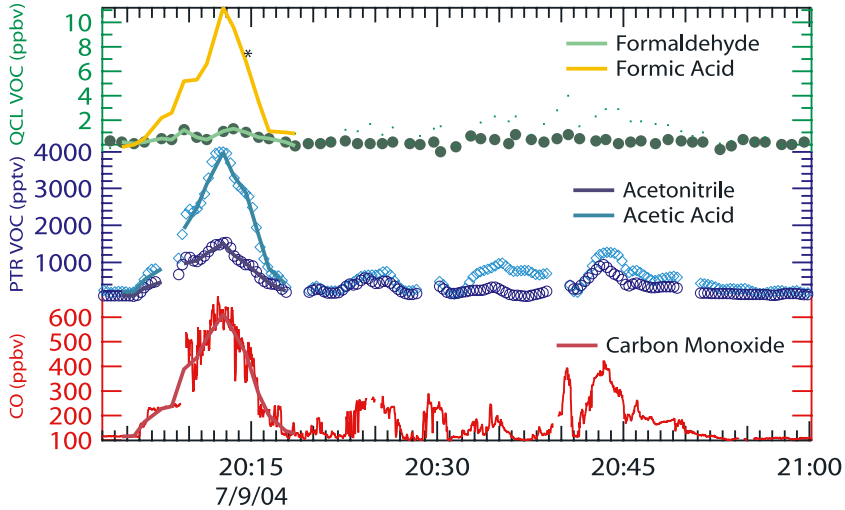

Figure 9. Fire plume intercept on 9 July 2004. The time series for each of measured concentrations have been computed for the PTR-MS time base. The solid lines have been used to compute enhancement ratios for this intercept.

Table 1. Formaldehyde and Formic Acid in the Fire Plume

	HCHO/CO, mmol mol^{-1}	HCOOH/CO, mmol mol^{-1}	Acetic/Formic Acid, mol mol^{-1}
9 Jul 2004, this work	2.4	20	0.37
Tabulated data from Table 5 of *Goode et al.* [2000, and references therein]	19 (16–26)[a]	7 (5–9)[a]	1.9 (1.4–2.1)[a]
Tabulated data from Table 1 of *Khare et al.* [1999, and references therein]			0.83 (0.62–1)[a]

[a]Values in parentheses are the first to third quartiles of the range of reported values.

[34] The concentration of HCOOH however, was somewhat greater in the aged plume (relative to CO) than has been previously observed in fire plumes [*Goode et al.*, 2000]. The comparison of these observations of the 9 July 2004 plume to previous findings is summarized in Table 1. The acetic acid to CO ratio in this plume [*de Gouw et al.*, 2006] is 2–2.5 times lower than the previous observations. The absolute HCOOH to CO ratio is greater than previous observations by a factor of 2.2–4. As a result, the ratio of acetic to formic acids in this plume is considerable lower than previous observations by about a factor of 5. The 9 July 2004 plume represents a single observation but the dramatic elevation of HCOOH suggests an active source, which could be the result of oxidation of other organic compounds, perhaps via HCHO, either in the gas phase or through heterogeneous processes [*Chameides and Davis*, 1983; *Jacob*, 1986].

3.3. Spectral Identification of HCHO and HCOOH

[35] One major advantage to the direct absorption sweep integration signal processing method we employ is the ability to unambiguously identify trace gas concentrations and potential interferences by spectral processing, even in the presence of overlapping molecular absorptions. This method of "fingerprint" fitting is particularly useful in the case of pulsed QC lasers when the laser line width is comparable to the molecular line widths at intermediate sampling pressure and spectral features can be overlapped to a greater degree than with Doppler limited spectroscopy. In the case of HCHO and HCOOH, which have similar mixing ratios and absorption line strengths, the spectral identification is crucial to obtaining the proper portioning between these two species in differing air masses.

[36] This point is illustrated in Figure 10, which shows spectra taken for two different air masses on separate aircraft flights. The specific times for each spectrum are indicated by an asterisk in Figures 8 and 9 for instances where the dominant mixing ratios are HCHO and HCOOH, respectively. The spectrum on the top (circles, offset for clarity), is a 1 s spectrum acquired during the isoprene oxidation event. Analysis of this spectrum indicates the air mass contained 5 ppbv of HCHO and less than 1 ppbv of HCOOH. The spectrum on the bottom (triangles) is the fire plume intercept where 7 ppbv of HCOOH and 1 ppbv of HCHO were measured. The fitting procedure unambigu-

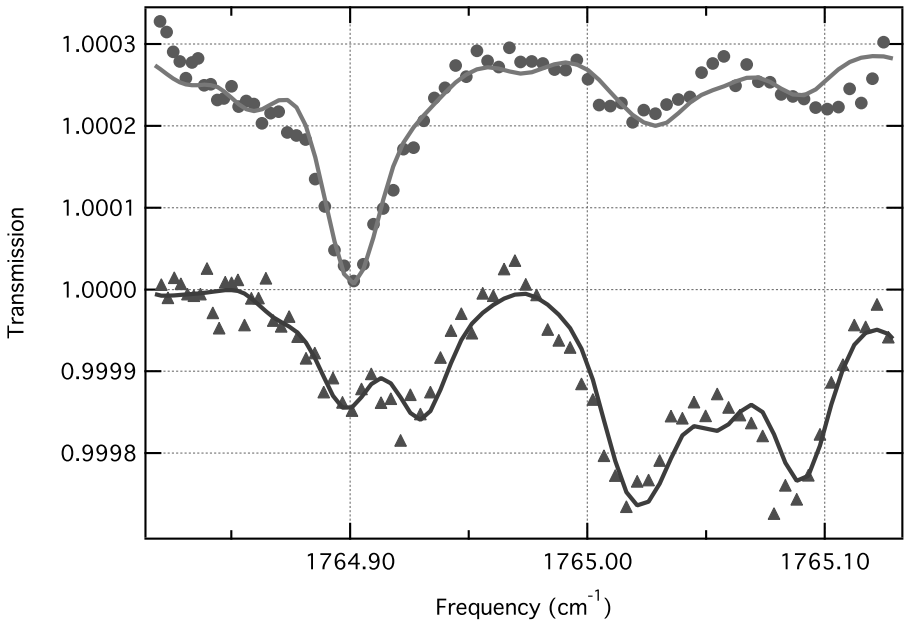

Figure 10. Transmission spectra acquired in flight. Two 1 s spectra are shown: The top data and fit were acquired on 3 July 2004 during the isoprene oxidation event, and the bottom data and fit were acquired during the fire plume intercept on 9 July 2004. Each of these fits are simultaneously fitting H_2O, HCHO and HCOOH in this wavelength region. These are the spectra represented by the asterisk mark on the time series in Figures 8 and 9.

Table 2. Large-Scale CO Plume Analysis for HCHO and CH_3CHO

Begin Time, LT	End Time, LT	J_{HCHO}, s^{-1}	HCHO/CO	HCHO/CH_3CHO
5 Jul 2004 1900	5 Jul 2004 1915	2.60E-05	0.044	4.2
9 Jul 2004 1530	9 Jul 2004 1600	4.00E-05	0.017	2.2
9 Jul 2004 1610	9 Jul 2004 1640	4.00E-05	0.01	2.8
9 Jul 2004 1740	9 Jul 2004 1820	5.50E-05	0.013	2.8
9 Jul 2004 2150	9 Jul 2004 2300		0.042	2.5
11 Jul 2004 2350	11 Jul 2004 2359	4.70E-07	0.018	3.3
12 Jul 2004 0045	12 Jul 2004 0100		0.042	6.9
31 Jul 2004 2250	31 Jul 2004 2354	1.00E-06	0.11	6.5
1 Aug 2004 0115	1 Aug 2004 0155		0.03	1.8
1 Aug 2004 0200	1 Aug 2004 0300		0.05	7.1
1 Aug 2004 0430	1 Aug 2004 0510	4.00E-09	0.05	6.1
3 Aug 2004 0230	3 Aug 2004 0330	1.00E-10	0.04	6.9
3 Aug 2004 0330	3 Aug 2004 0500	2.00E-09	0.016	2.9
7 Aug 2004 2115	7 Aug 2004 2350	3.00E-06	0.047	6.9
8 Aug 2004 0230	8 Aug 2004 0430	4.00E-10	0.028	4.7
9 Aug 2004 2310	9 Aug 2004 0030	4.00E-07	0.035	5.7
10 Aug 2004 0150	10 Aug 2004 0220		0.019	3
10 Aug 2004 0415	10 Aug 2004 0700	7.00E-10	0.024	4.4
14 Aug 2004 1900	14 Aug 2004 2100	2.10E-05	0.012	2.4
15 Aug 2004 1800	15 Aug 2004 2000	3.00E-05	0.027	1.9

ously identifies and quantifies each species in the presence of the other.

3.4. Urban Plume Analysis

[37] The detection sensitivity for HCHO from the flights following 11 July 2004 (features at wavelengths greater than 1765 cm^{-1}) was not as good as the measurements at 1765 cm^{-1}. Even with these noisier measurements, however, a striking correspondence is present on a timescale of tens of minutes between HCHO and CH_3CHO. Generally, the concentrations of each species were elevated over New York and the Philadelphia-Washington, D.C. corridor relative to the concentrations over Connecticut and central Pennsylvania. Correlations between HCHO, CH_3CHO and CO for the whole mission have been analyzed by choosing start and stop times on the basis of CO plumes. Though these decisions are arbitrary, the correlations in the resulting large-scale plumes may offer insight into the character of processed emissions from urban sources. The results of these defined times are summarized in Table 2. For each of the beginning and ending times in the table a HCHO to CO and HCHO to CH_3CHO ratio has been computed with a simple linear fit. When available, the average *J*-value for HCHO is also tabulated.

[38] Figure 11 shows a scatterplot of the data in Table 2. The pink shaded box encapsulates several HCHO/CH_3CHO emission ratios [*Herndon et al.*, 2006; *Rogers et al.*, 2006; *Schauer et al.*, 2002] The first point to be raised by Figure 11 is that the HCHO/CH_3CHO ratio determined in these large-scale ''plumes'' appears to fall into one of two groups. The night ratios are greater than the day ratios by $\sim$2. The photolysis rate for HCHO is greater than that of CH_3CHO so this is the likely driver of the difference in this ratio. The ratio of the rate constants for the loss of HCHO and CH_3CHO due to reaction with OH is $\sim$0.7 and furthermore the reaction of OH with CH_3CHO produces HCHO particularly in the presence of urban plume levels of NO which complicates a simple analysis of this ratio. This assessment would be better addressed with the use of a photochemical box model that can simultaneously estimate production and loss rates.

[39] The ratio of HCHO to CO found in the plumes identified in Table 2 and shown in Figure 11 appears to be greater than might be anticipated from direct transportation emissions. The data points contained in the blue shaded box are several HCHO/CO emission ratios [*Dasgupta et al.*, 2005; *Garcia et al.*, 2005; *Herndon et al.*, 2005a]. While the ratios of HCHO to CH_3CHO are plausibly associated with transportation sources, it is very unlikely that the measured HCHO (and therefore the CH_3CHO as well) are due to direct ''initial'' exhaust from internal combustion engines. The chosen ''plumes'' are biased toward being characteristically urban because CO was used as the primary criteria for their selection. The P3 flew many missions at night and it is presumed that the production and loss of HCHO via photochemical processes would be diminished for these flights. The HCHO to CO ratios encountered are not primary or initial HCHO in the tailpipe. There are several possibilities to explain this observation. One is that there are vast sources of direct HCHO which either have concomitant CO in a much greater ratio than that of internal combustion engine emissions, or do not have CO at all and are mixed with the urban transportation emissions. These plume events in this analysis are associated with urban events, and it is also possibly a biogenic VOC such as isoprene (and its seasonal dependence) is undergoing oxidation (even in the absence of photolytic cycling) as it is mixed with the urban emissions and the associated CO. Additional modeling will be required to fully address the results from Figure 11 and Table 2.

4. Conclusion and Future Work

[40] We have deployed a new generation infrared absorption spectrometer based on pulsed quantum cascade lasers to obtain simultaneous measurements of HCHO and HCOOH from the WP-3 aircraft during the NEAQS 2004. The instrument is smaller and more compact than instruments we have previously deployed using cryogenically cooled lead salt tunable diode lasers. During this initial deployment, we have observed HCHO and HCOOH in a variety of locations and times. When coupled with data

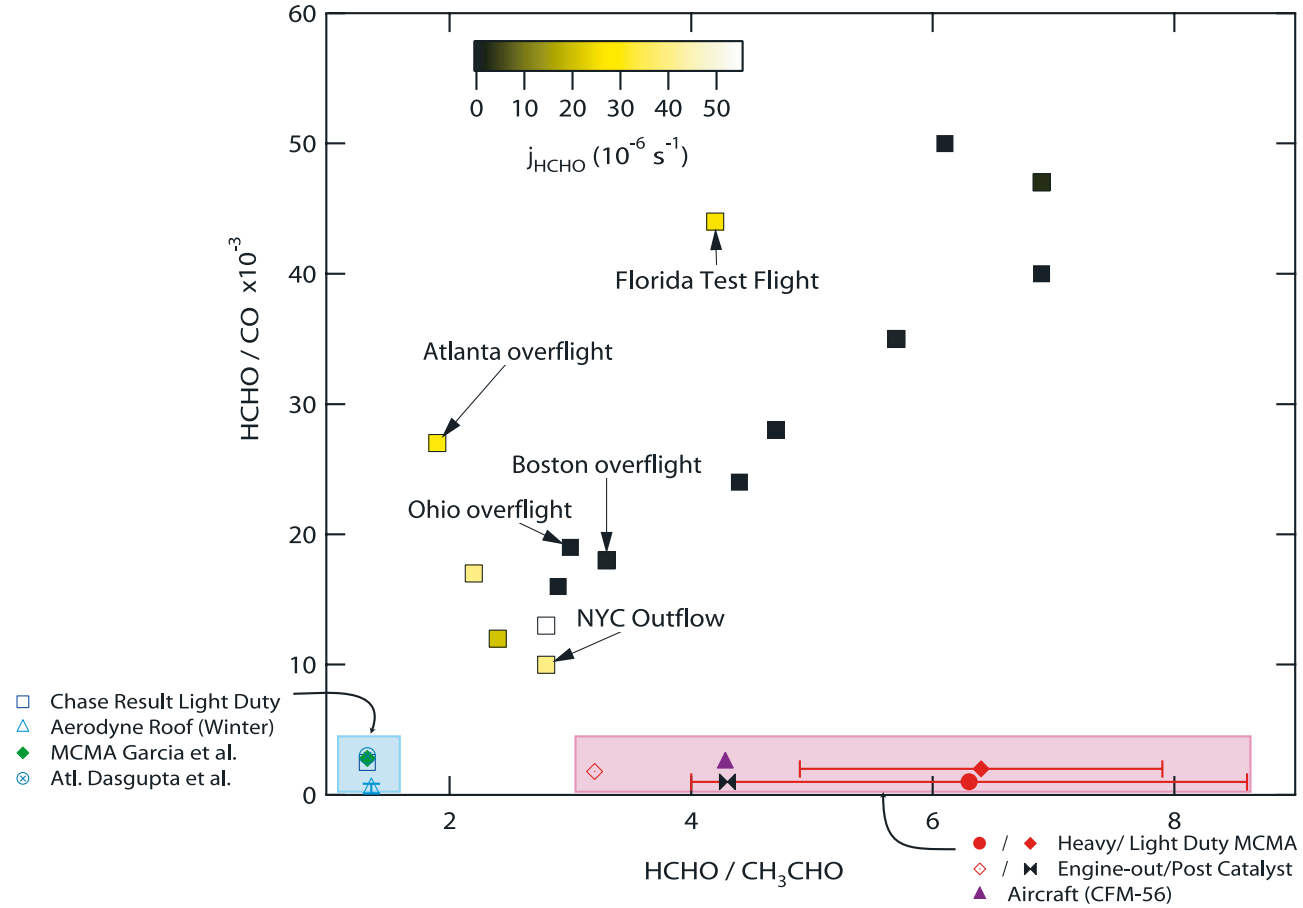

Figure 11. HCHO/CO and HCHO/CH_3CHO ratios. The squares with a black to yellow-white shading represent the in-flight urban correlation events from Table 2. The other data points on this figure correspond to either an HCHO/CO ratio (light blue box) or an HCHO/CH_3CHO ratio (pink box). The dark squares are indicative of night flights, while the yellow coloring is indicative of j_{HCHO} for the daytime flights.

from other instruments aboard the aircraft, these observations have revealed sources of HCHO and HCOOH from oxidation of isoprene, observations of enhanced HCOOH in aged forest fire plumes, and evidence of oxidation of secondary anthropogenic hydrocarbons in urban outflows. The data will be useful in continued attempts to model atmospheric hydrocarbon oxidation and secondary organic aerosol formation and removal.

[41] Future deployments of the instrument will have improvements that will lead to greater sensitivity and stability, particularly in the aircraft environment. Initial performance was limited by aircraft motion affecting the optical stability, even on the relatively short timescale between sample and background. We have identified and corrected several causes of instability with improved mechanical mounting and improved electronic design for laser driver and detector circuits.

[42] Advances in laser technology are expected to further enhance this approach to measurements of HCHO, HCOOH and other trace gases during airborne campaigns. Continuous wave quantum cascade lasers that operate without cryogenic cooling at room temperature are now available at selected wavelengths in the midinfrared [*Nelson et al.*, 2006]. The increased power, narrower line width, and higher spectral mode purity of these CW devices, compared to pulsed operation, will extend the sensitivity and selectivity of this method and allow autonomous routine sensing of these important trace gases from a wider variety of smaller aircraft platforms.

[43] **Acknowledgments.** Without Alan Fried's comprehensive assistance we would not have been able to fly. We would like to thank Tom Ryerson and Andy Neuman for extensive help with the zero air and inlet systems and Gerd Hubler for arranging our participation in the WP-3 deployment. We would like to thank John Holloway and Harald Stark for the specific use of their data. We gratefully acknowledge Jean Vander Auwera for his high-resolution formic acid data prior to publication. We thank the NOAA WP-3 crew and science collaborators from the NEAQS-ITCT 2004 campaign. We are very grateful to Bruce Daube, Bill Dube, and John Jayne for additional assistance with the instrument integration. We gratefully acknowledge the efforts of Guillaume Vandeputte, Yargo Bonetti, and Antoine Muller from ALPESLASERS for providing the primary and replacement quantum cascade lasers used in this deployment.

References

Andreae, M. O., and P. J. Crutzen (1997), Atmospheric aerosols: Biogeochemical sources and role in atmospheric chemistry, *Science*, *276*, 1052–1058.

Atkinson, R. (2000), Atmospheric chemistry of VOCs and NOx, *Atmos. Environ.*, *34*, 2063–2101.

Bakhirkin, Y. A., A. A. Kosterev, R. F. Curl, F. K. Tittel, D. A. Yarekha, L. Hvozdara, M. Giovannini, and J. Faist (2006), Sub-ppbv nitric oxide concentration measurements using cw thermoelectrically cooled quantum cascade laser-based integrated cavity output spectroscopy, *Appl. Phys. B*, *82*, 149–154.

Beck, M., D. Hofstetter, T. Aellen, J. Faist, U. Oesterle, M. Ilegems, E. Gini, and H. Melchior (2002), Continuous wave operation of a mid-infrared semiconductor laser at room temperature, *Science*, *295*, 301–305.

Blaser, S., D. A. Yarekha, L. Hvozdara, Y. Bonetti, A. Muller, M. Giovannini, and J. Faist (2005), Room-temperature, continuous-wave, single-mode quantum-cascade lasers at 5.4 μm, *Appl. Phys. Lett.*, *86*, 041109.

Chameides, W. L., and D. D. Davis (1983), Aqueous phase source of formic acid in clouds, *Nature*, *304*, 427–429.

Claeys, M., B. Graham, G. Vas, W. Wang, R. Vermeylen, V. Pashynska, J. Cafmeyer, P. Guyon, M. O. Andreae, P. Artaxo, and W. Maenhaut (2004), Formation of secondary organic aerosols through photooxidation of isoprene, *Science*, *303*, 1173–1176.

Dasgupta, P. K., J. Li, G. Zhang, W. T. Luke, W. A. McClenny, J. Stutz, and A. Fried (2005), Summertime ambient formaldehyde in five U.S. metropolitan areas: Nashville, Atlanta, Houston, Philadelphia and Tampa, *Environ. Sci. Technol.*, *39*, 4767–4783.

de Gouw, J. A., et al. (2006), Volatile organic compounds composition of merged and aged forest file plumes from Alaska and western Canada, *J. Geophys. Res.*, *111*, D10303, doi:10.1029/2005JD006175.

Finlayson-Pitts, B. J., and J. N. J. Pitts (2000), *Chemistry of the Upper and Lower Atmosphere*, Elsevier, New York.

Fried, A., S. Sewell, B. Henry, B. P. Wert, T. Gilpin, and J. R. Drummond (1997), Tunable diode laser absorption spectrometer for ground-based measurements of formaldehyde, *J. Geophys. Res.*, *102*, 6253–6266.

Fried, A., B. Henry, B. Wert, S. Sewell, and J. R. Drummond (1998), Laboratory, ground-based, and airborne tunable diode laser systems: Performance characteristics and applications in atmospheric studies, *Appl. Phys. B*, *67*, 317–330.

Fried, A., Y.-N. Lee, G. Frost, B. Wert, B. Henry, J. R. Drummond, G. Hubler, and T. Jobson (2002), Airborne CH_2O measurements over the North Atlantic during the 1997 NARE campaign: Instrument comparisons and distributions, *J. Geophys. Res.*, *107*(D4), 4039, doi:10.1029/2000JD000260.

Garcia, A. R., R. Volkamer, L. T. Molina, M. J. Molina, J. Samuelson, J. Mellqvist, B. Galle, S. C. Herndon, and C. E. Kolb (2005), Separation of emitted and photochemical formaldehyde in Mexico City using a statistical analysis and a new pair of gas-phase tracers, *Atmos. Chem. Phys. Disc.*, *5*, 11,583–11,615.

Goode, J. G., R. J. Yokelson, D. E. Ward, R. A. Susott, R. E. Babbitt, M. A. Davies, and W. M. Hao (2000), Measurements of excess O_3, CO_2, CO, CH_4, C_2H_4, C_2H_2, HCN, NO, NH_3, HCOOH, CH_3COOH, HCHO and CH_3OH in 1997 Alaskan biomass burning plumes by airborne Fourier transform infrared spectroscopy (AFTIR), *J. Geophys. Res.*, *105*, 22,147–22,166.

Heard, D. E., L. J. Carpenter, D. J. Creasey, J. R. Hopkins, J. D. Lee, A. C. Lewis, M. J. Pilling, P. W. Seakins, N. Carslaw, and K. M. Emmerson (2004), High levels of the hydroxy radical in the winter urban troposphere, *Geophys. Res. Lett.*, *31*, L18112, doi:10.1029/2004GL020544.

Herndon, S. C., J. H. Shorter, M. S. Zahniser, J. Wormhoudt, D. D. Nelson, K. L. Demerjian, and C. E. Kolb (2005a), Real-time measurements of SO_2, H_2CO and CH_4 emissions from in-use curbside passenger buses in New York City using a chase vehicle, *Environ. Sci. Technol.*, *39*, 7984–7990.

Herndon, S. C., L. Yongquan, D. D. Nelson, and M. S. Zahniser (2005b), Determination of line strengths for selected transitions in the nu2 band relative to the nu1 and nu5 bands of H_2CO, *J. Quant. Spectrosc. Radiat. Transfer*, *90*, 207–216.

Herndon, S. C., T. Rogers, E. J. Dunlea, R. C. Miake-Lye, and B. Knighton (2006), Hydrocarbon emissions from in-use commercial aircraft during airport operations, *Environ. Sci. Technol.*, *40*, 4406–4413.

Holloway, J. S., R. O. Jakoubek, D. D. Parrish, C. Gerbig, A. Volz-Thomas, S. Schmitgen, A. Fried, B. Wert, B. Henry, and J. R. Drummond (2000), Airborne intercomparison of vacuum-ultraviolet fluorescence and tunable diode laser absorption measurements of tropospheric carbon monoxide, *J. Geophys. Res.*, *105*, 24,251–24,261.

Houghton, J. T., Y. Ding, D. J. Griggs, M. Noguer, P. J. van der Linden, X. Dai, K. Maskell, and C. A. Johnson (Eds.) (2001), *Climate Change 2001: The Scientific Basis—Contribution of Working Group I to the Third Assessment Report of the Intergovernmental Panel on Climate Change (IPCC)*, Cambridge Univ. Press, New York.

Humlicek, J. (1979), An efficient method for evaluation of the complex probability function: The Voigt function and its derivatives, *J. Quant. Spectrosc. Radiat. Transfer*, *21*, 309–313.

Humlicek, J. (1982), Optimized computation of the Voigt and complex probability function, *J. Quant. Spectrosc. Radiat. Transfer*, *27*, 437–444.

Jacob, D. J. (1986), Chemistry of OH in remote clouds and its role in the production of formic acid and peroxymonosulfate, *J. Geophys. Res.*, *91*, 9807–9826.

Jacob, D. J., and S. Wofsy (1988), Photochemistry of biogenic emissions over the Amazon forest, *J. Geophys. Res.*, *93*, 1477–1486.

Jimenez, R., S. C. Herndon, J. H. Shorter, D. D. Nelson Jr., J. B. McManus, and M. Zahniser (2005), Atmospheric trace gas measurements using a dual quantum-cascade laser mid-infrared absorption spectrometer, *Proc. SPIE Int. Soc. Opt. Eng.*, *5738*, 318–331.

Khare, P., N. Kumar, K. M. Kumari, and S. S. Srivastava (1999), Atmospheric formic and acetic acids: An overview, *Rev. Geophys.*, *37*, 227–248.

Li, S.-M., K. G. Anlauf, H. A. Wiebe, and J. Bottenheim (1994), Estimating primary and secondary production of HCHO in eastern North America based on gas-phase measurements and principal component analysis, *Geophys. Res. Lett.*, *21*, 669–672.

Mason, S. A., R. J. Field, R. J. Yokelson, M. A. Kochivar, M. R. Tinsley, D. E. Ward, and W. M. Hao (2001), Complex effects arising in smoke plume simulations due to inclusion of direct emissions of oxygenated organic species from biomass combustion, *J. Geophys. Res.*, *106*, 12,527–12,539.

Matsunaga, S. N., C. Wiedinmyer, A. B. Guenther, J. J. Orlando, T. Karl, D. W. Toohey, J. P. Greenberg, and Y. Kajii (2005), Isoprene oxidation products are a significant atmospheric aerosol component, *Atmos. Chem. Phys. Disc.*, *5*, 11,143–11,156.

McManus, J. B., D. D. Nelson, S. C. Herndon, J. H. Shorter, M. S. Zahniser, S. Blaser, L. Hvozdara, A. Muller, M. Giovannini, and J. Faist (2006), Comparison of cw and pulsed operation with a TE-cooled quantum cascade infrared laser for detection of nitric oxide at 1900 cm−1, *Appl. Phys. B.*, *85*, 235–241, doi:10.1007/s00340-006-2407-7.

Miyoshi, A., S. Hatakeyama, and N. Washida (1994), OH radical-initiated photoxidation of isoprene: An estimate of global CO production, *J. Geophys. Res.*, *99*, 18,779–18,787.

Moeskops, B. W. M., S. M. Cristescu, and F. J. M. Harren (2006), Sub-part-per-billion monitoring of nitric oxide by use of wavelength modulation spectroscopy in combination with a thermoelectrically cooled, continuous-wave quantum cascade laser, *Opt. Lett.*, *31*, 823–825.

Molina, M. J., A. V. Ivanov, S. Trakhtenberg, and L. T. Molina (2004), Atmospheric evolution of organic aerosol, *Geophys. Res. Lett.*, *31*, L22104, doi:10.1029/2004GL020910.

Nelson, D. D., J. S. Shorter, J. B. McManus, and M. S. Zahniser (2002), Sub-part-per-billion detection of nitric oxide in air using a thermoelectrically cooled mid-infrared quantum cascade laser spectrometer, *Appl. Phys. B*, *75*, 343–350.

Nelson, D. D., J. B. McManus, S. Urbanski, S. Herndon, and M. S. Zahniser (2004), High precision measurements of atmospheric nitrous oxide and methane using thermoelectrically cooled mid-infrared quantum cascade lasers and detectors, *Spectrochim. Acta A*, *60*, 3325–3335.

Nelson, D. D., J. B. McManus, S. C. Herndon, J. H. Shorter, M. S. Zahniser, S. Blaser, L. Hvozdara, A. Muller, M. Giovannini, and J. Faist (2006), Characterization of a near-room-temperature, continuous-wave quantum cascade laser for long-term, unattended monitoring of nitric oxide in the atmosphere, *Opt. Lett.*, *31*, 2012–2014.

Neuman, J. A., T. B. Ryerson, L. G. Huey, R. O. Jakoubek, J. B. Nowak, C. Simons, and F. C. Fehsenfeld (2003), Calibration and evaluation of nitric acid and ammonia permeation tubes by UV optical absorption, *Environ. Sci. Technol.*, *37*, 2975–2981.

Orzechowska, G., and S. E. Paulson (2005), Photochemical sources of organic acids. 1. Reaction of ozone with isoprene, propene and 2-butenes under dry and humid conditions using SPME, *J. Phys. Chem. A*, *109*, 5358–5365.

Palmer, P. I., D. J. Jacob, A. M. Fiore, R. V. Martin, K. V. Chance, and T. P. Kurosu (2003), Mapping isoprene emissions over North America using formaldehyde column observations from space, *J. Geophys. Res.*, *108*(D6), 4180, doi:10.1029/2002JD002153.

Rasmussen, R. A. (1972), What do the hydrocarbons from trees contribute to air pollution?, *J. Air Pollut. Control Assoc.*, *22*, 537–543.

Rogers, T. M., et al. (2006), On-road measurements of volatile organic compounds in the Mexico City metropolitan area using proton transfer reaction mass spectrometry, *Int. J. Mass Spectrom.*, *252*, 26–37.

Ryerson, T. B., L. G. Huey, and F. C. Fehsenfeld (1999), Design and initial characterization of an inlet for gas-phase NOy measurements from aircraft, *J. Geophys. Res.*, *104*, 5483–5492.

Schauer, J. J., M. J. Kleeman, G. R. Cass, and B. R. T. Simoneit (2002), Measurement of emission from air pollution sources. 5 C1-C32 Organic compounds from gasoline-powered motor vehicles, *Environ. Sci. Technol.*, *36*, 1169–1180.

Sprengnether, M., K. L. Demerjian, N. M. Donahue, and J. G. Anderson (2002), Product analysis of the OH oxidation of isoprene and 1,3-butadiene in the presence of NO, *J. Geophys. Res.*, *107*(D15), 4268, doi:10.1029/2001JD000716.

Stohl, A., C. Forster, S. Eckhardt, N. Spichtinger, H. Huntrieser, J. Heland, H. Schlager, S. Wilhelm, F. Arnold, and O. Cooper (2003), A backward modeling study of intercontinental pollution transport using aircraft measurements, *J. Geophys. Res.*, *108*(D12), 4370, doi:10.1029/2002JD002862.

Trainer, M., E. J. Williams, D. D. Parrish, M. P. Buhr, E. J. Allwine, H. H. Westberg, F. C. Fehsenfeld, and S. C. Lui (1987), Models and observations of the impact of natural hydrocarbons on rural ozone, *Nature*, *329*, 705–707.

Tuazon, E. C., and R. Atkinson (1990), Product study of the gas-phase reaction of isoprene with OH radical in the presence of NOx, *Int. J. Chem. Kinet.*, *22*, 1221–1236.

von Kuhlmann, R., M. G. Lawrence, P. J. Crutzen, and P. J. Rasch (2003), A model for studies of tropospheric ozone and nonmethane hydrocarbons: Model evaluation of ozone-related species, *J. Geophys. Res.*, *108*(D23), 4729, doi:10.1029/2002JD003348.

Wagner, V., C. Schiller, and H. Fischer (2001), Formaldehyde measurements in the marine boundary layer of the Indian Ocean during the 1999 INDOEX cruise of the R/V *Ronald H. Brown*, *J. Geophys. Res.*, *106*, 28,528–28,538.

Went, F. W. (1960), Blue hazes in the atmosphere, *Nature*, *187*, 641–643.

Wert, B. P., A. Fried, B. Henry, and S. Cartier (2002), Evaluation of inlets used for the airborne measurement of formaldehyde, *J. Geophys. Res.*, *107*(D13), 4163, doi:10.1029/2001JD001072.

Yu, J. S., A. Evans, S. Slivken, S. R. Darvish, and M. Razeghi (2005), Short wavelength ($\lambda \sim 4{:}3$ μm) high-performance continuous-wave quantum-cascade lasers, *IEEE Photon. Technol. Lett.*, *17*, 1154–1156.

Zahniser, M. S., D. D. Nelson, J. B. McManus, and P. L. Kebabian (1995), Measurement of trace gas fluxes using tunable diode laser spectroscopy, *Philos. Trans. R. Soc. London, Ser. A*, *351*, 371–382.

Zhang, D., W. Lei, and R. Zhang (2002), Mechanism of OH formation from ozonolysis of isoprene: Kinetics and product yields, *Chem. Phys. Lett.*, *358*, 171–179.

Zhao, J., R. Zhang, E. C. Fortner, and S. W. North (2004), Quantification of hydroxycarbonyls from OH-isoprene reactions, *J. Am. Chem. Soc.*, *126*, 2686–2687.

J. A. de Gouw and C. Warneke, Earth System Research Laboratory, NOAA, Boulder, CO 80305, USA.

S. C. Herndon, J. B. McManus, D. D. Nelson Jr., J. Shorter, and M. S. Zahniser, Aerodyne Research Inc., Billerica, MA 01821, USA. (herndon@aerodyne.com)

R. Jiménez, Department of Earth and Planetary Sciences, Harvard University, Cambridge, MA 02138, USA.